Materials Science and Engineering A 399 (2005) 43–48

MATERIALS SCIENCE & ENGINEERING A

www.elsevier.com/locate/msea

X-ray microbeam measurements of subgrain stress distributions in polycrystalline materials

G.E. Ice*, B.C. Larson, J.Z. Tischler, W. Liu, W. Yang

Oak Ridge National Laboratory, P.O. Box 2008, Bldg. 4500S, MS-6118, Oak Ridge, TN 37831-6118, USA

Abstract

Three-dimensional (3D) measurements of strain tensor distributions with subgrain resolution are now possible due to an emerging class of instrumentation: the 3D X-ray crystal microscopes. These instruments combine ultra-intense synchrotron X-ray sources and advanced X-ray optics to probe polycrystalline materials with submicron spatial resolution. By employing polychromatic X-ray beams and a virtual pinhole camera method, called differential aperture microscopy, 3D distributions of the local crystalline phase, orientation (local texture) and elastic and plastic strain tensor distributions can be measured with resolution below the grain size of most materials. The elastic strain tensor elements can typically be determined with uncertainties less than 100 ppm in brittle materials. Orientations can be quantified to $\sim 0.01^\circ$ and the local unpaired dislocation density can be measured in ductile materials. Efforts are underway to improve the spatial resolution and increase the depth probed. Because the 3D X-ray crystal microscope is a penetrating nondestructive tool, it is ideal for studies of mesoscale structural evolution in materials. The unprecedented information that can be obtained with this new class of instrumentation is certain to advance our understanding of the materials physics underpinning the behavior of polycrystalline materials.
Published by Elsevier B.V.

Keywords: X-ray microbeam; Polycrystalline materials; Strain tensor

1. Introduction

Although the behavior of most materials is dependent on inhomogeneities with mesoscopic length scales of 0.1–10 μm, until recently no nondestructive tool existed with both the spatial resolution and the penetrating ability to study true three-dimensional (3D) mesoscopic structural evolution. Now an emerging class of instrumentation is opening up this new frontier. The so-called 3D X-ray crystal microscope on beamline 34-i.d. at the advanced photon source provides unprecedented spatially resolved measurements of crystalline phase, local texture (orientation), elastic and plastic strain. Stress in particular, is a key driving force for the evolution of mesoscale structure in materials and has long been associated with aging and other changes in mesoscale structure [1,2]. Yet the materials physics of how local stress evolves in materials, and how local inhomogeneities affect materials behavior is still elusive; experimental guidance has been limited because three-dimensional stress distribution maps with mesoscopic spatial resolution have been difficult or impossible to obtain. Nevertheless, there is compelling evidence of the importance of stress/strain inhomogeneities in materials. For example, in powder diffraction measurements, it is well known, that the measured strain depends on the crystallographic plane that is examined [3]. This is a consequence of unequal stress loading between grains with different orientations and recent theoretical work has been devoted to interpret the measured strains from many families of planes in order to accurately determine average stress [4,5]. Similarly, broadening of diffraction peaks is associated with local stress/strain fluctuations termed microstress, to distinguish it from average or macrostress [4,5].

The 3D X-ray crystal microscope measures the total local stress tensor within a small volume. The total stress is a superposition of type I (macroscopic stress); type II (intercrystalline fluctuations about type I stresses due to misorientation and crystalline anisotropy); type III (intra-crystalline stresses). In general, engineers have concentrated on type I—macroscopic stresses—that describe an ensemble average

* Corresponding author. Tel.: +1 865 574 2744; fax: +1 865 574 7659.
E-mail address: icege@ornl.gov (G.E. Ice).

0921-5093/$ – see front matter. Published by Elsevier B.V.
doi:10.1016/j.msea.2005.02.035

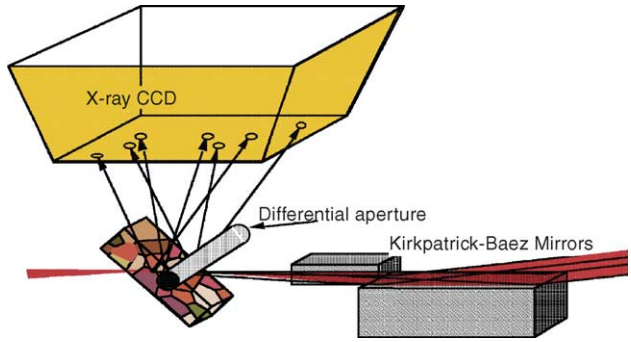

Fig. 1. Schematic of the 3D X-ray crystal microscope. The incident X-ray beam is focused by nondispersive Kirkpatrick–Baez mirrors to a submicron spot on the sample. A differential aperture cuts through the diffracted radiation to identify the source of the diffracted intensity along the probe beam. The diffracted pattern is measured by an X-ray sensitive CCD area detector.

over a small volume of the material that preserves force balance. Type I stress can be determined by integrating the local stress measured by the 3D X-ray crystal microscope. Types II and III stresses can then be recovered by subtracting the type I contribution from the locally measured stress distribution.

A schematic of the 3D X-ray crystal microscope [6–8] is shown in Fig. 1. In a typical experiment, a polychromatic X-ray beam impinges on a nondispersive (focus independent of wavelength) Kirkpatrick–Baez mirror pair. The total-external-reflection elliptical mirrors focus the X-ray beam to a submicron spot on the sample [9]. The sample is rastered in the X-ray beam by a precision three-axis stage to select a line through the sample for analysis. The Laue patterns generated by each voxel illuminated by the X-ray beam are collected by an X-ray sensitive CCD. The overlapping Laue patterns from each voxel along the X-ray beam are separated by a differential aperture that scans across the surface of the sample [7]. From the separated Laue patterns, it is possible to determine the phase, and orientation of crystalline structure within each voxel. In addition, it is often possible to determine the deviatoric strain tensor and/or the deformation tensor.

In order to determine dilatation (hydrostatic) strain, an additional step is required: the energy of one reflection must be determined. The reflection energy is determined by inserting a nondispersive monochromator into the X-ray beam and tuning to the energy of on the Bragg/Laue reflection. The monochromator can be tuned over an ∼10 keV range without displacing the X-ray probe focal position [10].

Closely related to the 3D X-ray crystal microscope, are triangulation methods that have been used on X-ray microscopes at the ESRF [11,12] and SSRL [13], and on an earlier prototype of the 3D X-ray crystal microscope at the APS [14]. Triangulation can be significantly faster than differential aperture microscopy, but is less amenable to automation and has lower intrinsic resolution.

2. Theory

White-beam Laue diffraction is a standard crystallographic method used to determine crystal orientation [15–17]. Although it has major advantages for microdiffraction, Laue diffraction is rarely used to measure strain/stress because the precision of most Laue instruments is low compared to modern monochromatic beam diffractometers, and because the unit cell *volume* cannot be determined with a standard Laue measurement. Nevertheless, with suitable instrumentation, the Laue method can be used to precisely determine the orientation (local texture) of individual grains and their deviatoric strain (shape deformation of the unit cell). Laue diffraction can also be extended, by measuring the energy of one or more reflections to determine the hydrostatic strain and combined with the deviatoric strain, the full local strain tensor. In order to measure strain *distributions*, a large number of measurements must be collected which favors automated methods.

Single crystal diffraction directly measures the average local strain tensor of the crystal through the orientation of the unit cell and the distortion of the lattice parameters from their (unstrained) values. This is distinct from powder diffraction averages and allows for direct calculation of the local elastic stress. Consider, for example, a unit cell with lattice parameters a_i and α_i and a Cartesian coordinate system $\boldsymbol{u}_i$, which is attached to the crystal. We adopt a notation where the vector $\boldsymbol{a}_1$ is coincident with the $\boldsymbol{u}_1$ axis, $\boldsymbol{a}_2$ is in the $\boldsymbol{u}_1\boldsymbol{u}_2$ plane, and $\boldsymbol{u}_3$ is perpendicular to the $\boldsymbol{u}_1\boldsymbol{u}_2$ plane (see Fig. 2). Similar notation has been adopted by previous authors [17–20].

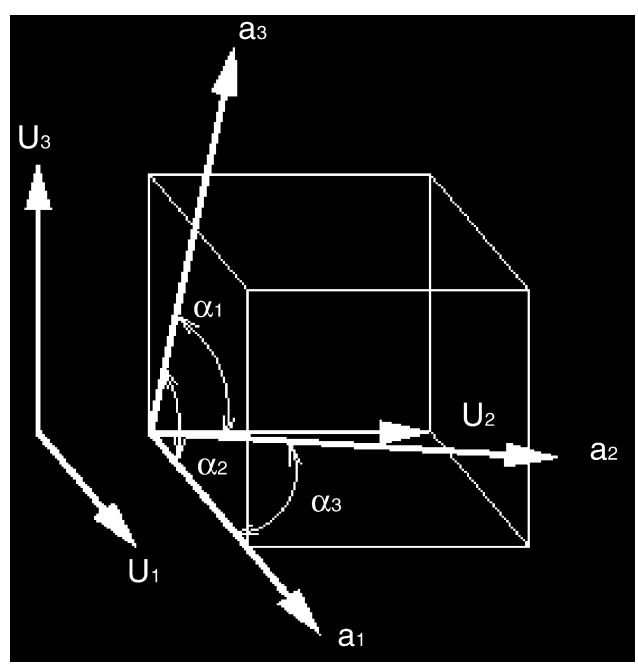

Fig. 2. Co-ordinates attached to the real-space unit cell. Note that $\boldsymbol{u}_1 = \boldsymbol{a}_1/|\boldsymbol{a}_1|$; $\boldsymbol{u}_3 = \boldsymbol{a}_1 \times \boldsymbol{a}_2/\boldsymbol{a}_1||\boldsymbol{a}_2|\sin\alpha$; $\boldsymbol{u}_2 = \boldsymbol{a}_3 \times \boldsymbol{a}_1$.

A position in the crystal can be specified either by a vector in the Cartesian coordinates $\boldsymbol{v}_{\mathrm{u}}$ or by a vector with unit cell coordinates $\boldsymbol{v}$. The transformation from unit cell coordinates to Cartesian coordinates is given by:

$$\boldsymbol{v}_{\mathrm{u}} = \mathbf{A}\boldsymbol{v}$$

where

$$\mathbf{A} = \begin{pmatrix} a_1 & a_2\cos\alpha_3 & a_3\cos\alpha_2 \\ 0 & a_2\sin\alpha_3 & -a_3\sin\alpha_2\cos\beta_1 \\ 0 & 0 & 1/b_3 \end{pmatrix}. \quad (1)$$

Here, the β_is and b_is are the reciprocal lattice parameters for the unit cell.

A vector position attached to a crystal can move due to rigid body translation of the crystal, due to rigid body rotation of the crystal, or due to distortion of the crystal lattice (strain) [21]. The average strain of a measured unit cell can be determined by comparing the measured unit cell parameters to the unit cell parameters of undistorted material. Let $\mathbf{A}_{\mathrm{Meas}}$ be the matrix, which converts a measured vector $\boldsymbol{v}$ into the measured crystal Cartesian coordinates. Let $\mathbf{A}_0$ be the matrix for an *unstrained* unit cell, which converts $\boldsymbol{v}$ into the Cartesian reference frame of the measured (strained) crystal. To ensure that there is no rigid body translation between the measured unit cell and the unstrained unit cell, the origin of the unit cell vectors are made coincident. For convenience, we assume $\boldsymbol{a}_1$ of the unstrained unit cell lies along the $\boldsymbol{u}_1$ axis and $\boldsymbol{a}_2$ of the unstrained unit cell to lie in the $\boldsymbol{u}_1\boldsymbol{u}_2$ plane.

A position vector $\boldsymbol{v}_{\mathrm{u}}$ in the unit cell coordinates is found in the measured-crystal Cartesian coordinate reference frame at position $\mathbf{A}_0\boldsymbol{v}$ for the unstrained case and at position $\mathbf{A}_{\mathrm{Meas}}\boldsymbol{v}$ for the strained case. With this definition, for the matrices $\mathbf{A}_{\mathrm{Meas}}$ and $\mathbf{A}_0$ there is a transformation matrix $\mathbf{T}$, which maps from unstrained to strained vectors:

$$\mathbf{A}_{\mathrm{Meas}}\boldsymbol{v} = \mathbf{T}\mathbf{A}_0\boldsymbol{v} \quad (2)$$

The transformation matrix can include both distortion and rotation terms and for unstrained crystals $\mathbf{T} = \mathbf{I}$. From the definition of the strain tensor, ε_{ij}, the strain tensor in the measured-crystal Cartesian-coordinate reference frame is given by:

$$\varepsilon_{ij} = \frac{\mathbf{T}_{ij} + \mathbf{T}_{ij}}{2} - \mathbf{I}_{ij}. \quad (3)$$

The strain tensor in the crystal reference frame can be converted to a laboratory reference frame or to a sample reference frame by using a rotation matrix $\mathbf{R}$:

$$\varepsilon_{ij}^{\mathrm{Sample}} = \mathbf{R}\varepsilon_{ij}\mathbf{R}^{-1} \quad (4)$$

The strain tensor of Eq. (3) contains both a hydrostatic strain (dilatation) and a distortion strain term. With the hydrostatic strain, $\Delta/3$ defined as the mean strain component along each Cartesian axis, Eq. (3) can be written in terms of the two components:

$$\varepsilon_{ij} = \begin{pmatrix} \varepsilon_{11} - \frac{\Delta}{3} & \varepsilon_{12} & \varepsilon_{13} \\ \varepsilon_{12} & \varepsilon_{22} - \frac{\Delta}{3} & \varepsilon_{23} \\ \varepsilon_{13} & \varepsilon_{23} & \varepsilon_{33} - \frac{\Delta}{3} \end{pmatrix} + \begin{pmatrix} \frac{\Delta}{3} & 0 & 0 \\ 0 & \frac{\Delta}{3} & 0 \\ 0 & 0 & \frac{\Delta}{3} \end{pmatrix} \quad (5)$$

where $\Delta = \varepsilon_{11} + \varepsilon_{22} + \varepsilon_{33}$.

Here, the first term is the distortion term and the second term is the dilatation term. With microdiffraction measurements, it is important to retain the full (nine parameter) information contained in the crystal strain tensor *and* local grain orientation; the stress tensor can be determined from the strain tensor and the anisotropic single crystal elastic constants (stiffness modulii) [21].

Laue measurements directly determine the local crystallographic orientation and deviatoric strain tensor elements but not the dilatational component Δ. For this component the energy of one reflection must be identified as described above.

3. Instrumentation

Several experimental innovations are needed for a practical 3D X-ray crystal microscope. For example, elliptical total-external-reflection mirrors with slope errors less than ~1 μrad are used to produce a small X-ray beam. These mirrors are made by differentially depositing Au onto X-ray quality spherical substrates [9]. The small compact mirrors produced by this method are easy to align and very stable. We typically find that no alignment is required for months of beam operation. A special monochromator is also essential for this class of instrumentation [10]. We use a small-offset two-crystal $Si_{1\,1\,1}$ monochromator that is based on flex pivot rotations. This instrument has been found to be very stable and reproducible and allows for tuning over thousands of electron volts with less than ±1 eV uncertainty.

Particularly innovative is the use of a differential aperture to decode the origin of the intensity along the incident X-ray beam [7]. As shown in Fig. 3, as the X-ray beam penetrates the sample it generates diffraction from the subgrains along its path. If a high Z wire is passed near the surface of the sample, it occludes some of the X-rays generated along the X-ray path. The wire position can be incremented by submicron steps parallel to the sample surface. The difference between the diffraction pattern before and after a small move arises from rays passing near the front or back edge of the wire. Because the position of the wire can be determined

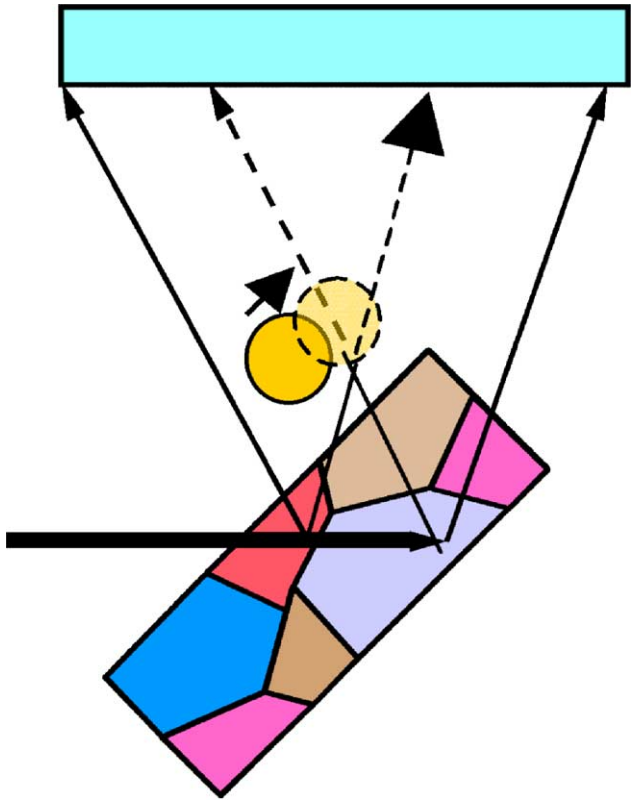

Fig. 3. Schematic showing the principle behind differential aperture microscopy. Rays passing near the leading or trailing edge of the wire show large changes in transmission as the wire is moved. The origin of the intensity can be triangulated back to the source.

with high precision, and because of the large relative distance from wire-to-detector compared to from beam-to-wire, the intensity at each pixel can be decoded to determine where it originated along the beam. This method is called differential aperture microscopy.

4. Research directions

The 3D X-ray crystal microscope can both address long-standing problems of fundamental interest to materials physics, and provide specific insights and directions to materials and process development programs. Examples of fundamental issues that can be addressed by the 3D X-ray crystal microscope include the role of stress on grain growth and anisotropic deformation. For example, experiments are currently underway to understand the role of 3D stress in grain growth and coarsening of Al. Here, the morphology and grain-boundary motions of individual buried Al grains can be monitored and correlated to local elastic stress. Similarly measurements of deformation in polycrystalline Ni include characterization of the elastic stress distribution. Here, there is an interest in correlating local stress with local plastic deformation, subgrain evolution and grain rotation. Although these growth and deformation experiments are just

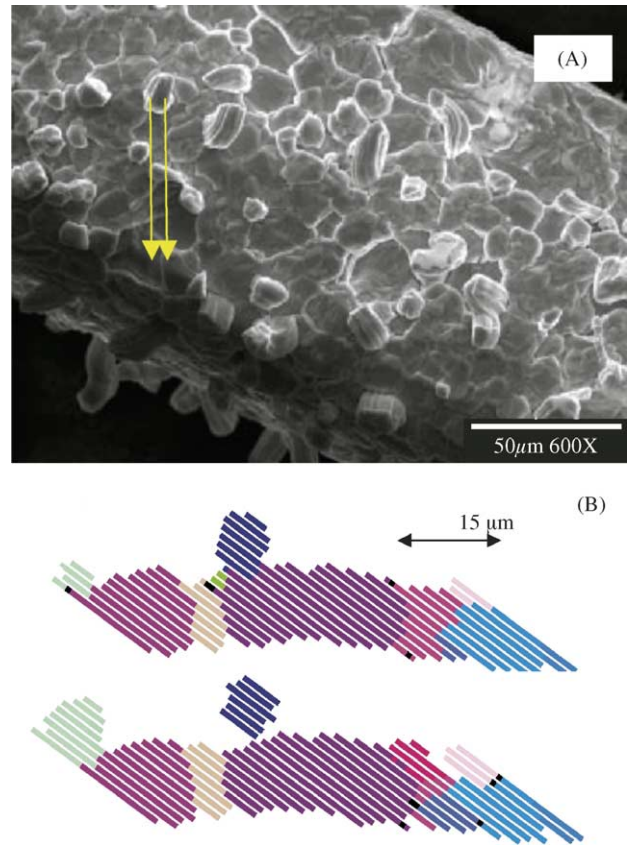

Fig. 4. (A) SEM image of a Sn film showing whiskers. The yellow lines indicate the approximate surface region probed by the 3D X-ray crystal microscope. (B) False color maps indicating local cry stall ographic orientation in two adjacent slices—2 μm apart. Whiskers are clearly visible, projecting out of the surface of the film near the left edge and center of the images.

now underway, they hold great promise as they can provide direct guidance to growth and deformation computer simulation codes. To illustrate the unprecedented experimental opportunities offered by the 3D X-ray crystal microscope we describe two experiments currently underway.

4.1. Whisker development in Sn

The growth of Sn whiskers is a major problem hindering the development of lead-free solders. As illustrated in Fig. 4A, whiskers develop from even thin Sn surface layers. Despite long-standing interest in the growth of Sn whiskers, there is continuing controversy over the key mechanisms causing Sn whisker growth. To test various models there are three key questions: (1) What is the orientation of whiskers as compared to average texture? (2) What is the nature of the grain-boundary network near whiskers? (3) What is the stress distribution in and near whiskers? The 3D X-ray crystal microscope is an ideal tool for addressing these key questions. Recent measurements with 2D X-ray microscopy have begun to address the question of the average Sn texture compared with the orientation of whiskers [22]. Recent measurements with the 3D X-ray crystal microscope allow for

a three-dimensional view of the whisker that includes the interrelationship of the grain with its near-neighbor environment. In particular, as illustrated in Fig. 4B, whisker crystallographic orientation can be related to the crystallographic orientation of neighbor grains and the grain boundaries can be classified. In addition, by using differential aperture microscopy, the strain tensor within and near to a Sn whisker can be measured. Since the local Sn environment is single crystal, strain can be directly related to the local stress. Measurements to characterize the stress distribution within a single whisker are underway.

4.2. Grain-boundary stress behavior

Experimental measurements of grain-boundary properties are an important area where the 3D X-ray crystal microscope can provide new information that is essential for accurate modeling of polycrystalline materials behavior. Recent measurements with the 3D X-ray crystal microscope have demonstrated the ability to precisely characterize grain boundary type. In these measurements, the grain-boundary morphology is measured to ∼1 μm and the crystallographic orientation of the neighbor grains are determined within ∼0.01. Based on the misorientation between the two neighbor grains and the grain-boundary normal, the grain boundary is classified according to coincidence site lattice theory. For example, as illustrated in Fig. 5, the surface normal of the grain boundary can be determined from the position of three grain-boundary intercepts *if* the surface is assumed to be locally flat. Measurements of local stress distributions near the grain boundary can be used to model the elastic/plastic response of the grain boundary to local stress. Of particular interest is the ability of grain boundaries of various types to carry shear loads. Measurements of the shear load capacity of various grain boundaries will provide essential new information for modelers. Experiments following anisotropic plastic deformation are currently underway, and measurements of elastic strain distributions near grain boundaries are planned.

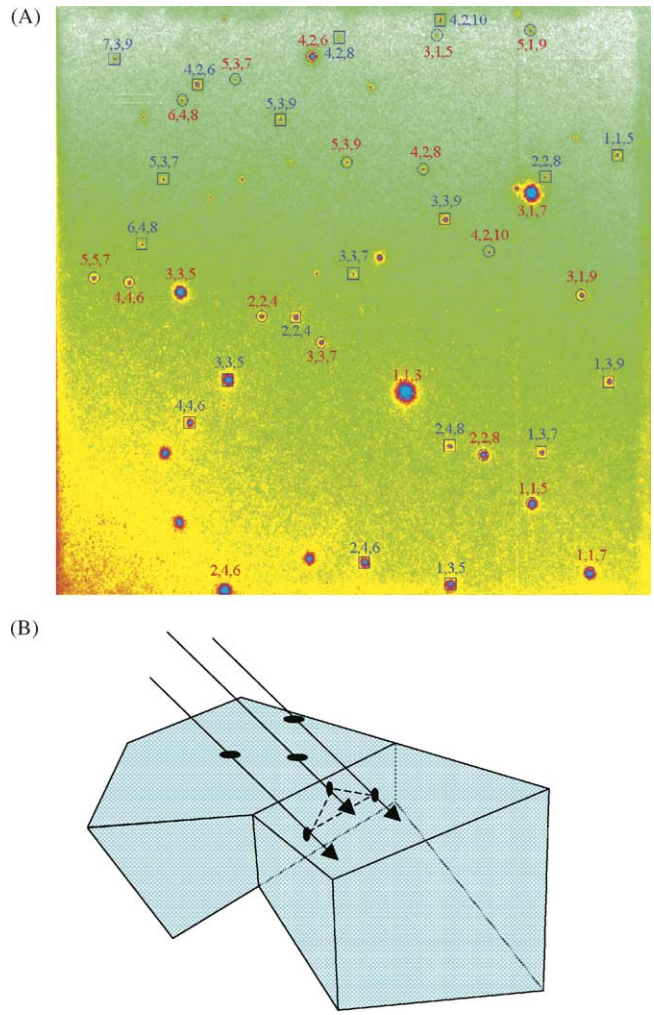

Fig. 5. (A) Near a grain boundary, the Laue patterns from two grains are observed. The patterns can be indexed to precisely determine the orientation of each grain. As shown in the indexed patterns from two nickel grains, many reflections are recovered even from this simple fcc metal; (B) with differential aperture microscopy, the 3D position of the grain boundary/X-ray beam intersect can be determined. Assuming a locally planar grain boundary, three noncolinear (linearly independent) intersects determine a grain-boundary normal.

5. Future developments

The ability to map out statistically significant sample volumes is limited primarily by detector readout speed. Our CCD camera can readout in about 2 s, whereas the exposure time needed for good diffraction images varies from about 1 to 50 ms. Even faster exposure times are possible with evolving X-ray optics. We estimate that better mirrors and the removal of a graphite commissioning window from the beamline could decrease exposure times by a factor of 10. It is therefore quite reasonable to imagine an optimized 3D X-ray crystal microscope, which can collect images at ∼20–200 Hz. This will accelerate our data acquisition by more than 2 orders of magnitude, will qualitatively improve measurements of mesoscale dynamics, and will allow for the study of larger volumes with better spatial resolution.

There is also a need to look deeper into materials and/or to study materials with even finer grain size. Efforts are now underway to develop nanofocusing optics with ∼50 nm spatial resolution. This will allow for measurements on materials with characteristic structure an order of magnitude smaller than currently possible. Efforts are also underway to extend the microdiffraction X-ray method to neutron probes where grains far below the sample surface can be probed.

Although new directions of 3D X-ray crystal microscopy are still emerging, it is clear that this new class of instrumentation opens important opportunities for the study of materials. The unique ability to study strain/stress distributions in 3D with submicron resolution is certain to advance our understanding of materials.

Acknowledgements

Work sponsored by the Division of Materials Sciences through the Oak Ridge National Laboratory. Oak Ridge National Laboratory (ORNL) is operated by UT-Battelle, LLC, for the U.S. Department of Energy under contract DE-AC05-00OR22725. Work in part on Unicat beamline 34-ID. at the Advanced Photon Source (APS), which is supported by the University of Illinois at Urbana-Champaign, Materials Research Laboratory (U.S. DOE, the State of Illinois-IBHE-HECA, and the NSF), and by the Oak Ridge National Laboratory (U.S. DOE under contract with UT-Battelle LLC). The APS is supported by the U.S. DOE, Basic Energy Sciences, Office of Science under contract No. W-31-109-ENG-38.

References

[1] F.J. Humphreys, M. Hatherly, Recrystallization and Related Annealing Phenomena, Elsevier Science Inc., 1995.
[2] E.C. Oliver, et al., Ecrs 6: Proceedings of the 6th European Conference on Residual Stresses, 2002, pp. 489–494.
[3] J.W.L. Pang, T.M. Holden, T.E. Mason, Acta Mater. 46 (5) (1998) 1503–1518.
[4] T.M. Holden, R.A. Holt, J.W.L. Pang, Metall. Mater. Trans. A 33 (3) (2002) 749–755.
[5] T.M. Holden, C.N. Tome, R.A. Holt, Metall. Mater. Trans. A 29 (12) (1998) 2967–2973.
[6] J.-S. Chung, G.E. Ice, J. Appl. Phys. 86 (1999) 5249–5256.
[7] B.C. Larson, Wenge Yang, G.E. Ice, J.D. Budai, J.Z. Tischler, Nature 415 (2002) 887–890.
[8] G.E. Ice, B.C. Larson, Adv. Eng. Mater. 2 (2000) 643–646.
[9] G.E. Ice, J.S. Chung, J.Z. Tischler, A. Lunt, L. Assoufid, Rev. Sci. Inst. 71 (2000) 2635–2639.
[10] G.E. Ice, J.S. Chung, W. Lowe, E. Williams, J. Edelman, Rev. Sci. Inst. 71 (2000) 2001–2006.
[11] H.F. Poulsen, S.F. Nielsen, E.M. Lauridsen, S. Schmidt, R.M. Suter, U. Lienert, L. Margulies, T. Lorentzen, D. Juul Jensen, J. Appl. Cryst. 34 (2001) 751–756.
[12] U. Lienert, R. Martins, S. Grigull, M. Pinkerton, H.F. Poulson, A. Kvick, Mater. Res. Soc. 590 (2000) 241.
[13] C.R. Patterson II, K.I. Ignatiev, A. Guvenilir, J.S. Haase, R. Morano, Z.U. Rek, S.R. Stock, Mater. Res. Soc. 590 (2000) 253.
[14] B.C. Larson, N. Tamura, J.S. Chung, G.E. Ice, J.D. Budai, J.Z. Tischler, W. Yang, H. Weiland, W.P. Lowe, Mater. Res. Soc. Symp. 590 (2000) 247.
[15] I.A. Sheremetyev, A.V. Turbal, Y.M. Litvinov, M.A. Mikhailov, Nucl. Inst. Meth. A308 (1991) 451–455.
[16] R.B.G. Ravelli, A.M.F. Hezemans, H. Krabbendam, J. Kroon, J. Appl. Cryst. 29 (1996) 270–278.
[17] H.R. Wenk, F. Heidelbach, D. Chateigner, F. Zontone, J. Synch. Rad. 4 (1997) 95–101.
[18] W.R. Busing, H.A. Levy, Acta Cryst. 22 (1967) 457–464.
[19] A.L. Patterson, International Tables for X-ray Crystallography, vol. II, Kynoch Press, Birmingham, 1959, p. 61.
[20] J.S. Rollett, Computing Methods in Crystallography, Pergamon Press, Oxford, 1965, pp. 22–23, 28–31.
[21] I.C. Noyan, J.B. Cohen, Residual Stress: Measurement by Diffraction and Interpellation, Springer-Verlag, New York, 1987.
[22] W.J. Choi, T.Y. Lee, K.N. Tu, N. Tamura, R.S. Celestre, A.A. MacDowell, Y.Y. Bong, L.G.T.T. Sheng, IEEE 52nd Electronic Component & Technology Conference Proceedings, IEEE Catalog number 02CH3734-5, San Diego, CA, 28–31 May, 2002, pp. 628–633, LBNL-51035.